



AALBORG UNIVERSITY
DENMARK

Aalborg Universitet

A New Buck-Boost AC/DC Converter with Two-Terminal Output Voltage for DC Nano-Grid

Li, Xiangkun; Wu, Weimin; Wang, Houqing; Gao, Ning; Chung, Henry Shu-hung; Blaabjerg, Frede

Published in:
Energies

DOI (link to publication from Publisher):
[10.3390/en12203808](https://doi.org/10.3390/en12203808)

Publication date:
2019

Document Version
Publisher's PDF, also known as Version of record

[Link to publication from Aalborg University](#)

Citation for published version (APA):

Li, X., Wu, W., Wang, H., Gao, N., Chung, H. S., & Blaabjerg, F. (2019). A New Buck-Boost AC/DC Converter with Two-Terminal Output Voltage for DC Nano-Grid. *Energies*, 12(20), Article 3808. <https://doi.org/10.3390/en12203808>

General rights

Copyright and moral rights for the publications made accessible in the public portal are retained by the authors and/or other copyright owners and it is a condition of accessing publications that users recognise and abide by the legal requirements associated with these rights.


- Users may download and print one copy of any publication from the public portal for the purpose of private study or research.
- You may not further distribute the material or use it for any profit-making activity or commercial gain
- You may freely distribute the URL identifying the publication in the public portal -

Take down policy

If you believe that this document breaches copyright please contact us at vbn@aub.aau.dk providing details, and we will remove access to the work immediately and investigate your claim.

Article

A New Buck-Boost AC/DC Converter with Two-Terminal Output Voltage for DC Nano-Grid

Xiangkun Li ¹, Weimin Wu ^{1,*}, Houqing Wang ¹, Ning Gao ¹, Henry Shu-hung Chung ² and Frede Blaabjerg ³ 

¹ Department of Electronic Engineering, Shanghai Maritime University, Shanghai 201306, China; yingsuna@outlook.com (X.L.); houqingok@163.com (H.W.); ngao@shmtu.edu.cn (N.G.)

² Department of Electronic Engineering, City University of Hong Kong, Hong Kong 999077, China; eeshc@cityu.edu.hk

³ Department of Energy Technology, Aalborg University, Aalborg DK-9220, Denmark; fbl@et.aau.dk

* Correspondence: wmwu@shmtu.edu.cn

Received: 7 August 2019; Accepted: 30 September 2019; Published: 9 October 2019



Abstract: Due to the development and deployment of renewable DC power sources and their inherent advantages for DC loads in applications, the DC nano-grid has attracted more and more research attentions; especially the topologies of AC/DC converters are increasingly studied. When designing an AC to DC converter for a DC nano-grid system, the grounding configuration, which determines the costs, the efficiency as well as the safety, plays an important role. A three-terminal output AC to DC converter based on united grounding configuration has been presented for DC nano-grid. However, it has to be pointed out that the three-terminal output DC nano-grid is not as popular as the two-terminal DC output one, due to the infrastructure consideration. This paper proposes a new Buck-Boost AC to DC converter with two-terminal output voltage for DC nano-grid. The operating principle, the steady-state analysis, and the small signal modelling for the proposed converter working in continuous conduction mode are presented in detail. A 220 V/50 Hz/800 W prototype was fabricated to verify the effectiveness of the proposed converter.

Keywords: buck-boost; converter; dc nano-grid; single inductor

1. Introduction

Due to the energy crisis and the environmental issues caused by the consumption of traditional fossil fuels, a large number of renewable power conversion systems are connected to low voltage AC distribution systems as distributed generators. Note that many renewable power sources generate DC energies, while more and more power loads show DC characteristics. Therefore, the DC nano-grids are put forward to be instead of the conventional AC microgrid due to the energy efficiency consideration [1,2], and become more and more attentions [3–13].

In order to flexibly utilize the DC power generated by the renewable energy sources, a bi-directional AC/DC converter is generally adopted as the interface between the DC nano-grid and the AC power system. However, in some places, due to a large number of dc loads, the power generated by the local renewable energy sources cannot meet the consumption of local DC loads, so the traditional AC grid needs to provide power to DC nano-grid and the interface works like a power factor correction rectifier [10].

Generally, for safety, household appliances need to be connected with ground line, whether in a DC nano-grid or a low-voltage AC grid [12–15]. When selecting the power converter between the DC nano-grid and the low-voltage AC grid, the grounding should be first addressed. Three basic types

of the grounding configurations for the DC nano-grid have been summarized in [10], including the united grounding, the virtual isolated grounding and the unidirectional grounding.

In [15–20], various AC to DC converters were reviewed and compared, but the suitable AC to DC converters based on the united grounding configuration for DC nano-grid application were not introduced. Thus, [10] introduced a dual Buck-Boost AC to DC converter for DC nano-grid based on the principle of Two-Switch Buck-Boost (TSBB) converter, which is a simplified cascade connection of the Buck and Boost converter. This transformerless Buck-Boost AC to DC converter has three-terminal DC outputs and the AC system is common-ground with the DC system. Due to the application of MOSFET switching devices, only one switch operates in the high frequency state at any time, the switching losses of this converter can be reduced a lot. In order to solve the imbalance of the three-terminal output voltages of the converter in [10], which may be due to the unbalanced loads, a coupled-inductor-based Buck-Boost AC to DC converter was proposed in [12]. And to further improve the efficiency of the converter in [12], a modified dual buck-boost AC/DC converter with self-balanced DC output voltages in [13] was proposed. All these techniques have accelerated the application of DC nano-grid. However, it has to be pointed out that the three-terminal output DC nano-grid is not as popular as the two-terminal DC output one, due to the infrastructure consideration. Hence, exploring a new topology of Buck-Boost AC to DC converter with only two-terminal DC output in DC nano-grid applications is very important and valuable.

In this study, as shown in Figure 1, a new transformerless Buck-Boost AC to DC converter is proposed by inserting an additional switched network into a TSBB converter. During the positive AC grid voltage, the proposed AC to DC converter operates like a TSBB converter. During the negative AC grid voltage, the proposed AC to DC converter operates like a single-switch Buck-Boost converter. The main merit of the proposed Buck-Boost AC to DC converter is that two-terminal DC output can be successfully achieved, while only a single DC inductor is required and its utilization factor is 100%, resulting in the reduction of size and cost.

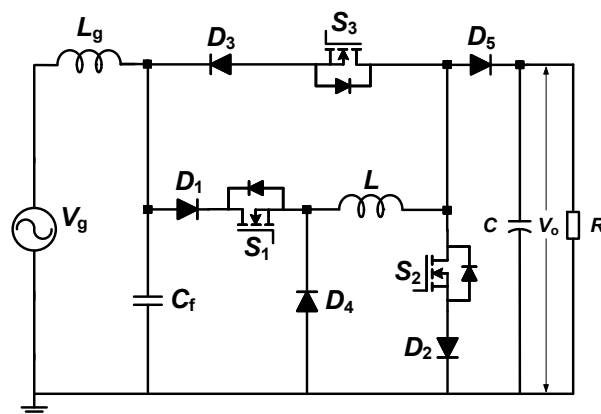


Figure 1. Proposed AC to DC converter with an inductor.

The rest of this paper is organized as follows. In Section 2, the structure of the new transformerless Buck-Boost AC to DC converter is proposed, while its operating principle is illustrated via the equivalent circuits in three working states. The steady-state characteristics of the converter are analyzed in Section 3. The small-signal model is derived, and control strategy of the proposed converter is introduced in Section 4. In order to confirm the theoretical analysis as well as the operating modes, an experimental prototype is developed, and the results are provided in Section 5. Finally, the conclusions are given in Section 6.

2. Proposed AC to DC Converter

2.1. Proposed Topology

Figure 1 shows the circuit configuration of the new transformerless Buck–Boost AC to DC converter, which consists of three power switches (S_{1-3}), five diodes (D_{1-5}), one DC inductor (L), two capacitors (filter capacitor C_f and electrolytic capacitor C) and one resistive load R . To facilitate the operating principle of the proposed AC to DC converter, the circuit can be simplified to the structure as shown in Figure 2.

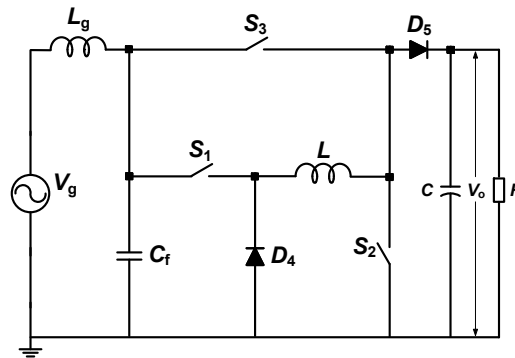


Figure 2. Simplified AC to DC converter with an inductor.

2.2. Operating Principle Description

According to the amplitude comparison between the output DC voltage of V_o and the AC grid voltage of V_g , as shown in Figure 3, the proposed converter has three working states in a line period. Since only one switch operates in high frequency state at any time, the switching power losses can be minimized. During the positive half period of AC grid voltage, the new Buck–Boost AC to DC converter is a TSBB converter. When $V_o \geq V_g$, the system works in the “Boost” state. S_1 is on, S_3 is off, S_2 works with high frequency and the equivalent circuits of the converter are depicted in Figure 4. When $V_o < V_g$, S_1 works with high frequency and the rest of the switches are off. The converter works like a pure “Buck” converter, where the equivalent circuits can be depicted in Figure 5.

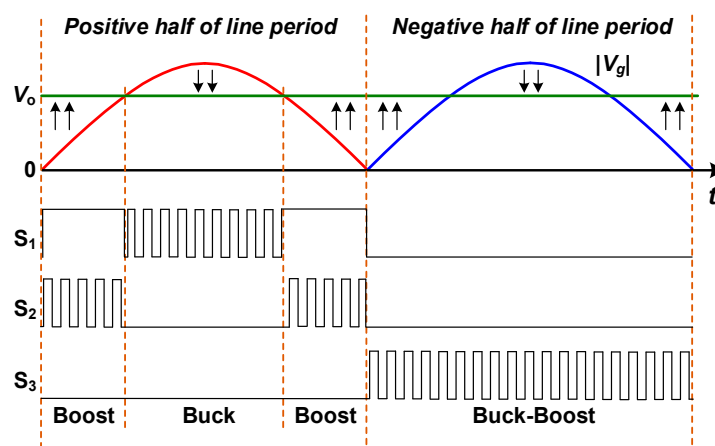


Figure 3. Operating states and gate signals of the proposed AC to DC converter.

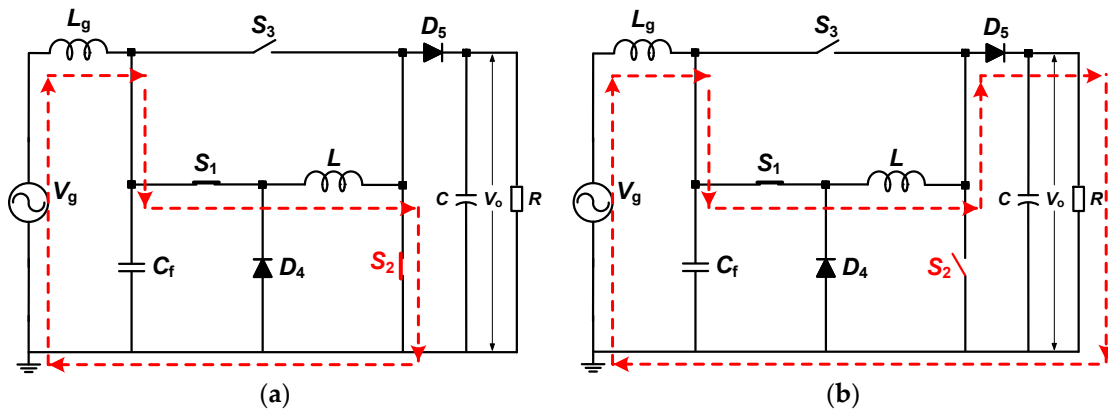


Figure 4. Equivalent circuits of the “Boost” state in the positive AC grid voltage: (a) Energy storing; (b) Energy releasing.

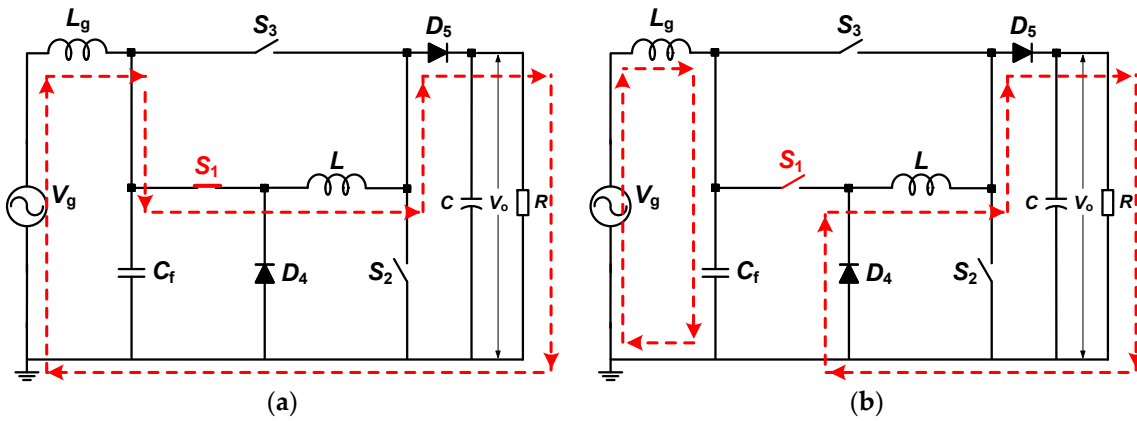


Figure 5. Equivalent circuits of the “Buck” state in the positive AC grid voltage: (a) Energy storing; (b) Energy releasing.

During the negative AC grid voltage, the proposed Buck-Boost AC to DC converter is a single-switch Buck-Boost converter. S_1 and S_2 are off, S_3 operates in high frequency state and the operating states are shown in Figure 6. When S_3 is on, the AC Source supplies the power to the DC inductor. When S_3 is off, the power stored in the inductor will be released to R , where the whole system works in the “Buck-Boost” state.

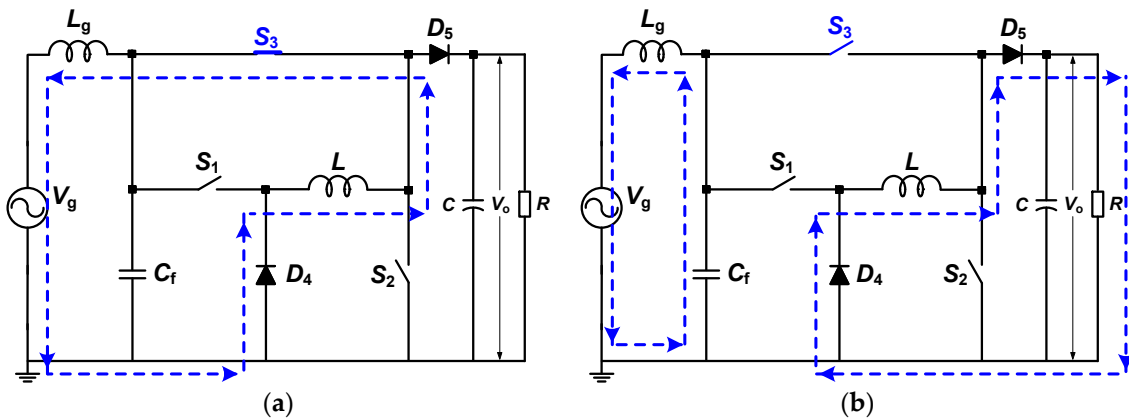


Figure 6. Equivalent circuits of the “Buck-Boost” state in the negative AC grid voltage: (a) Energy storing; (b) Energy releasing.

3. Steady-State Characteristics

3.1. Grid Current

The proposed converter works like a power factor correction circuit and the objective of the converter is to transfer the AC power to the DC load while synchronizing the input AC current with the AC grid voltage in phase. Therefore, the grid current can be expressed as:

$$i_g(t) = I_{g_peak} \sin(\omega t) \quad (1)$$

where I_{g_peak} is the peak amplitude of grid current.

3.2. Low Frequency Voltage of the Filter Capacitor

Since the inductance of the grid inductor is very small (micro-henry scale), the voltage drop and phase angle caused by the grid inductor are so small that they can be ignored. The voltage across the filter capacitor V_{C_f} is approximately equal to the grid voltage. It can be determined as:

$$v_{C_f}(t) \approx v_g(t) = V_{g_peak} \sin(\omega t) \quad (2)$$

where V_{g_peak} is the peak amplitude of grid voltage, ω is the angular frequency of grid voltage.

3.3. Duty Ratio

Figures 4–6 show the operating principle of the proposed converter via the equivalent circuits. The converter operates in “Boost” state, “Buck” state, and “Buck-Boost” state respectively. Thus, the duty ratio D can be expressed by:

$$D_{Boost}(t) = \frac{v_o - |v_g(t)|}{v_o} \quad (3)$$

$$D_{Buck}(t) = \frac{v_o}{|v_g(t)|} \quad (4)$$

$$D_{Buck-Boost}(t) = \frac{v_o}{v_o + |v_g(t)|} \quad (5)$$

It can be seen that when the DC output voltage is constant, the duty cycle varies with the grid voltage.

3.4. Low Frequency Current of the DC Inductor

When the converter works in “Boost” state, from Figure 4, it can be seen that the low frequency DC inductor current is the same as the grid current. Thus, the low frequency DC inductor current can be determined as:

$$i_L(t) = i_g(t) \quad (6)$$

When the converter operates in “Buck” state, the low frequency DC inductor current can be derived through the energy balance equation as:

$$i_L(t) = \frac{v_g(t) \cdot i_g(t)}{v_o} \quad (7)$$

When the converter operates in “Buck-Boost” state, as shown in Figure 6b, the energy stored in the DC inductor is transferred to the DC loads during the energy-releasing period. Assuming that the devices used in the converter are ideal, the relative power losses can be neglected. According to the energy balance equation, the output power is equal to the input power in a switching cycle when

the converter is operating in the steady state. Thus, the low frequency DC inductor current can be derived as:

$$i_L(t) = \frac{v_g(t) \cdot i_g(t)}{v_o(1 - D_{Buck-Boost}(t))} \quad (8)$$

3.5. High Frequency Current Ripple of the DC Inductor

Assume that the converter works in continuous conduction mode (CCM), during the energy-storing period, the current ripple of the DC inductor can be derived through the state equation, which can be expressed as:

$$v_L(t) = L \frac{\Delta i_L}{T_{ON}} \quad (9)$$

where $v_L(t)$ is the voltage across the DC inductor and T_{ON} is the turn-on time in a switching period. Thus, the high frequency current ripple of the DC inductor can be expressed as:

$$\Delta i_L(t) = \frac{v_L(t) \cdot D(t)}{L \cdot f_{SW}} \quad (10)$$

where D is the duty ratio, f_{SW} is the switching frequency.

As shown in Figure 4a, when the AC to DC converter works in “Boost” state, $v_L(t)$ and $v_g(t)$ are equal during the energy-storing period. The high frequency current ripple of the DC inductor can be expressed as:

$$\Delta i_{L_Boost}(t) = \frac{v_g(t) D_{_Boost}(t)}{L \cdot f_{SW}} \quad (11)$$

According to the Equations (3) and (11), the DC inductor current ripple $\Delta i_{L_Boost}(t)$ can be achieved as:

$$\Delta i_{L_Boost}(t) = \frac{v_g(t) \cdot (v_o - |v_g(t)|)}{L \cdot f_{SW} \cdot v_o} \quad (12)$$

Similarly, when the proposed converter works in “Buck” and “Buck-Boost” state, the DC inductor current ripple can be obtained as:

$$\Delta i_{L_Buck}(t) = \frac{(|v_g(t)| - v_o) \cdot v_o}{L \cdot f_{SW} \cdot |v_g(t)|} \quad (13)$$

$$\Delta i_{L_Buck-Boost}(t) = \frac{|v_g(t)| \cdot v_o}{L \cdot f_{SW} \cdot (v_o + |v_g(t)|)} \quad (14)$$

It can be observed from Equations (12)–(14) that the amplitude of DC inductor current ripple is time varying with the grid voltage.

3.6. High Frequency Voltage Ripple of the Filter Capacitor

When the converter works in “Boost” state, the high frequency voltage ripple of filter capacitor can be neglected since the filter capacitor current is very small. When the converter works in “Buck” state and “Buck-Boost” state, the voltage ripple of filter capacitor is caused by discharge from the grid inductor. During the energy-releasing period, the current of the filter capacitor is equal to the grid inductor current. In a short switching cycle, the grid current can be regarded as a constant current. Therefore, the voltage ripple peak to peak value of the filter capacitor $\Delta v_{C_f}(t)$ can be defined as:

$$i_{C_f}(t) = C_f \frac{\Delta v_{C_f}(t)}{T_{OFF}} \quad (15)$$

where i_{C_f} is the current of filter capacitor.

$$\Delta v_{C_f}(t) = \frac{i_g(t) \cdot (1 - D(t))}{C_f \cdot f_{SW}} \tag{16}$$

By putting Equations (4) and (5) into Equation (16) respectively, the voltage ripple of the filter capacitor can be obtained when the converter operates in “Buck” state and “Buck-Boost” state as:

$$\Delta v_{C_f_Buck}(t) = \frac{i_g(t) \cdot (|v_g(t)| - v_o)}{C_f \cdot f_{SW} \cdot |v_g(t)|} \tag{17}$$

$$\Delta v_{C_f_Buck-Boost}(t) = \frac{i_g(t) \cdot |v_g(t)|}{C_f \cdot f_{SW} \cdot (v_o + |v_g(t)|)} \tag{18}$$

From Equations (17) and (18), it can be seen that the value of high frequency voltage ripple of the filter capacitor is time varying with the grid voltage and grid current.

4. Small Signal Modelling and Controller Design

According to the circuit analysis in Section 2, the working states of proposed AC to DC converter include “Boost”, “Buck” and “Buck-Boost”. When the converter operates in “Boost” and “Buck” state, the small signal modeling had been presented and analyzed in [12,21], and the control versus the grid current transfer functions of “Boost”, and “Buck” stages are deduced as Equations (19) and (20) respectively as:

$$\left. \frac{\hat{i}_{Lg}(s)}{\hat{d}(s)} \right|_{\substack{\hat{v}_g(s) = 0 \\ \hat{v}_o(s) = 0}} = \frac{V_o}{s^3 L_g L C_f + s(L_g + L)} \tag{19}$$

$$\left. \frac{\hat{i}_{Lg}(s)}{\hat{d}(s)} \right|_{\substack{\hat{v}_g(s) = 0 \\ \hat{v}_o(s) = 0}} = \frac{s L I_L + D V_{C_f}}{s^3 L_g L C_f + s(D_{S1}^2 L_g + L)} \tag{20}$$

where, D_{S1} is the duty cycle of the switch S_1 .

Thus, in this paper, the control analysis in the “Buck-Boost” stage will be focused on.

During the “Buck-Boost” state, the equivalent circuits have been depicted in Figure 6. To simplify the analysis, the effects of the semiconductors have been ignored. Figure 6a,b show the equivalent circuits when S_3 is on during $[t, t + DT_s]$ and off during $[t + DT_s, t + T_s]$, respectively. The state equation can be deduced as followings:

$$\begin{bmatrix} L & 0 & 0 \\ 0 & L_g & 0 \\ 0 & 0 & C_f \end{bmatrix} \frac{d}{dt} \begin{pmatrix} i_L(t) \\ i_g(t) \\ v_{C_f}(t) \end{pmatrix} = A_{on} \begin{pmatrix} i_L(t) \\ i_g(t) \\ v_{C_f}(t) \end{pmatrix} + B_{on} \begin{pmatrix} v_o(t) \\ v_g(t) \\ 0 \end{pmatrix} \tag{21}$$

where, $A_{on} = \begin{bmatrix} 0 & 0 & 1 \\ 0 & 0 & -1 \\ -1 & 1 & 0 \end{bmatrix}$, $B_{on} = \begin{bmatrix} 0 & 0 & 0 \\ 0 & 1 & 0 \\ 0 & 0 & 0 \end{bmatrix}$.

$$\begin{bmatrix} L & 0 & 0 \\ 0 & L_g & 0 \\ 0 & 0 & C_f \end{bmatrix} \frac{d}{dt} \begin{pmatrix} i_L(t) \\ i_g(t) \\ v_{C_f}(t) \end{pmatrix} = A_{off} \begin{pmatrix} i_L(t) \\ i_g(t) \\ v_{C_f}(t) \end{pmatrix} + B_{off} \begin{pmatrix} v_o(t) \\ v_g(t) \\ 0 \end{pmatrix} \tag{22}$$

where, $A_{off} = \begin{bmatrix} 0 & 0 & 0 \\ 0 & 0 & -1 \\ 0 & 1 & 0 \end{bmatrix}$, $B_{off} = \begin{bmatrix} -1 & 0 & 0 \\ 0 & 1 & 0 \\ 0 & 0 & 0 \end{bmatrix}$.

Using the average state small signal modeling method and assuming that the AC grid source brings no disturbance and the electrolytic capacitor C is large enough that the output voltage ripple and fluctuation can be ignored during one switching period, the control versus grid current transfer function can be derived as:

$$\left. \frac{\hat{i}_{Lg}(s)}{\hat{d}(s)} \right|_{\substack{\hat{v}_g(s) = 0 \\ \hat{v}_o(s) = 0}} = \frac{sLI_L - D_{S3}(V_{C_f} + V_o)}{s^3L_gLC_f + s(D_{S3}^2L_g + L)} \tag{23}$$

where, D_{S3} is the duty cycle of the switch S_3 .

The control to grid current transfer functions in three operating states indicate that the proposed converter is a typical third order system. The controller design of typical third order system has been fully analyzed in [22–26], so more detailed control design will not be given in this paper.

Figure 7 depicts the whole control block diagram of proposed AC to DC converter, where the AD sampling signals include the output DC voltage of V_o , the grid voltage of V_g and the grid current i_g . Double control loops with Proportional Integral (PI) controllers are adopted in the system, where the outer loop is to control the output DC voltage and the inner loop is to make the grid inductor current to track the sinusoidal waveform and synchronize with the AC grid voltage. Besides, the gate signals of switches are obtained by comparison of modulated signals and carrier signal.

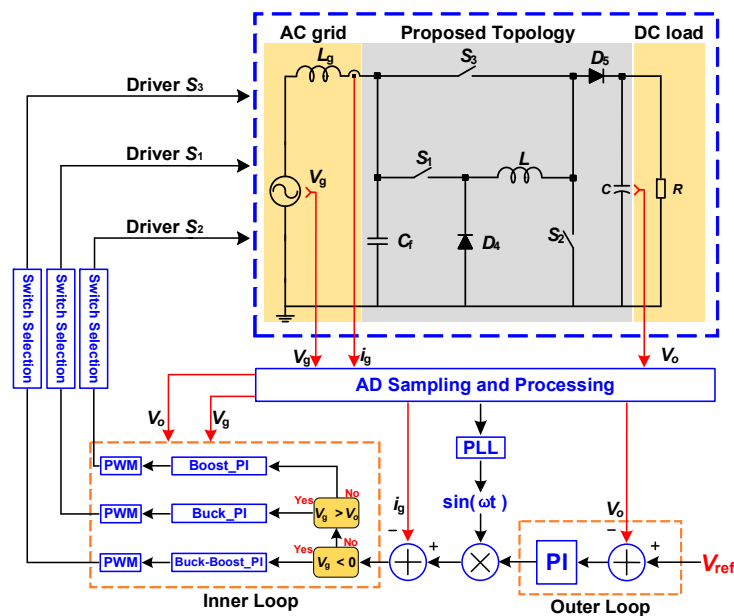


Figure 7. Controller block diagram.

5. Experimental Results

Experiments based a 220 V/800 W/50 Hz prototype have been carried out in the laboratory to validate the effectiveness and performance of the proposed topology. The photograph of the prototype is shown in Figure 8. The AC grid voltage is generated by a programmable AC source (Chroma 6530). The efficiency of the converter is measured by a digital power meter. Table 1 shows the specification and key parameters of the prototype. The selected devices used in the prototype are listed in Table 2. Limited by the laboratory hardware resources, the core EE110 is adopted in DC inductor and grid inductor. And the core material used in inductors is PC40.

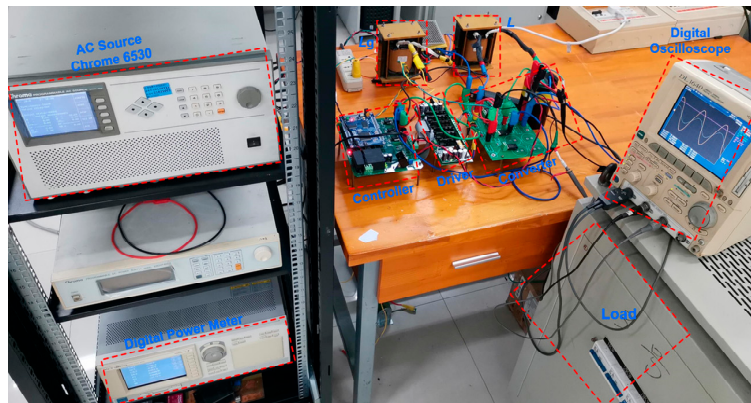


Figure 8. Photograph of the experimental setup.

Table 1. Parameters of the proposed converter.

Parameters	Value
Grid inductance L_g	0.6 mH
Filter capacitance C_f	2 μ F
DC inductance L	1.2 mH
DC output capacitor C	5600 μ F
Grid voltage V_g	220 V
Grid frequency f_0	50 Hz
DC output voltage V_o	200 V
Input power P_{in}	750 W
Switching frequency f_{sw}	40 kHz

Table 2. Selected devices in the prototype.

Devices	Type
Switches S_1 – S_3	IPW65R041CFD
Diodes D_1 – D_5	IDW30G65C5
Capacitor C_f	IKC CBB22
Core of the inductors	EE110

Figure 9 shows the gate signals of switches when the reference value of the DC output voltage (V_o) is set to 200 V and the AC input grid voltage (V_g) is set to 220 V/50 Hz ($V_{g_peak} = 311$ V). When the proposed converter works in “Boost”, “Buck” and “Buck-Boost” states, the gate signals of switches in high frequency are shown in Figure 10 respectively. It can be seen that the states of switches meet with the principle analyzed in Section 2.

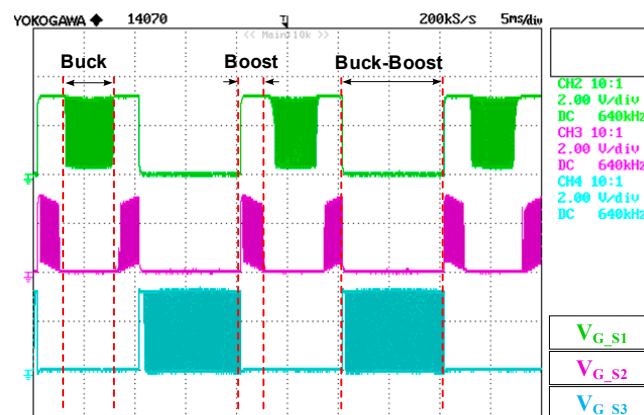


Figure 9. Measured Gate signals of MOSFETS when $V_o = 200$ V, and $V_{g_peak} = 311$ V.

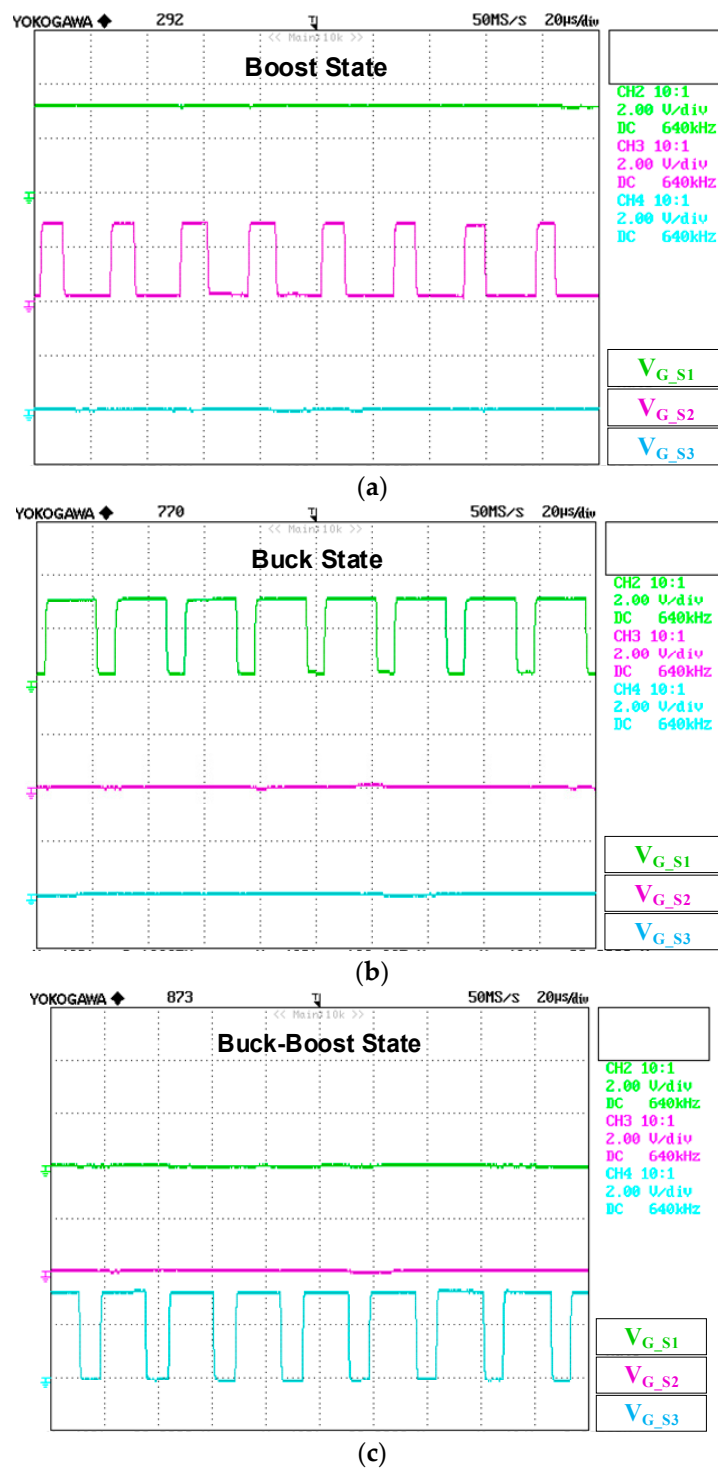


Figure 10. Measured Gate signals of MOSFETS when the proposed converter works in (a) Boost state; (b) Buck state; (c) Buck-Boost state.

Figures 11 and 12 show the experimental results when the AC input peak voltage (V_{g_peak}) is smaller than the DC output voltage (V_o), where the grid AC voltage is set to 110 V/50 Hz ($V_{g_peak} = 155$ V) and the reference value of the DC output voltage V_o is set to 200 V. Figure 11 shows the measured AC grid voltage ($V_g(t)$), the output DC voltage (V_o), and the grid inductor current ($i_g(t)$). Figure 12 shows the filter capacitor voltage ($V_{C_f}(t)$) and the DC inductor current ($i_L(t)$). During “Buck-Boost” operation, the maximum filter capacitor voltage ripple is about 28 V, which is consistent with Equation (18).

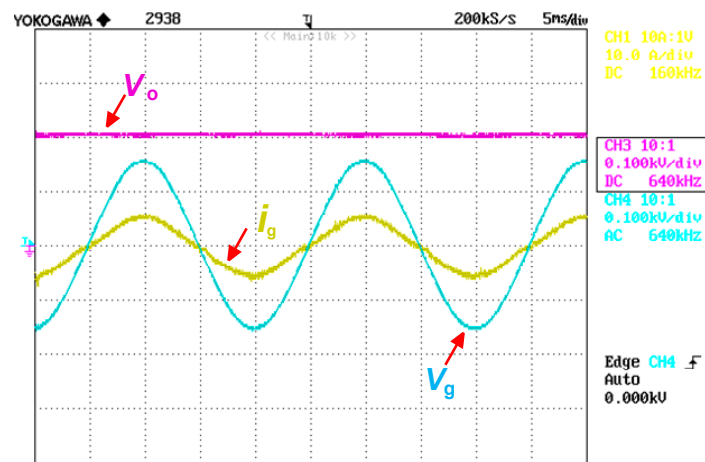


Figure 11. Measured input AC voltage ($V_g(t)$), the output DC voltage (V_o), and the input grid current i_g , when $V_o = 200$ V, $V_g = 110$ V, $R = 110 \Omega$.

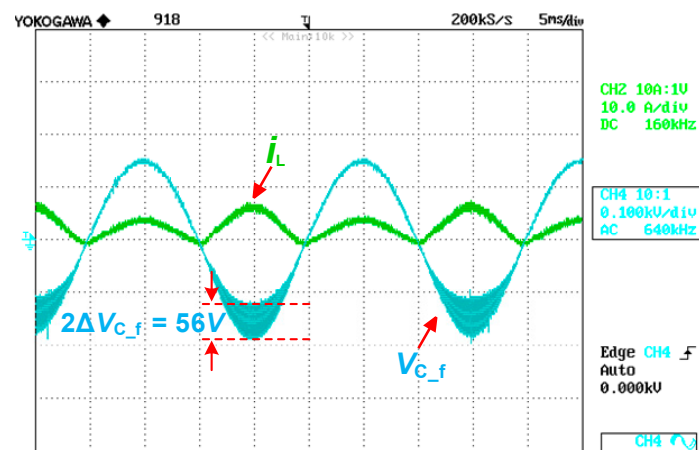


Figure 12. Measured capacitor voltage ($V_{C_f}(t)$) and the dc inductor current i_L , when $V_o = 200$ V, $V_g = 110$ V, $R = 110 \Omega$.

Figures 13 and 14 show the experimental results when the grid voltage is set to 220 V/50 Hz ($V_{g_peak} = 311$ V) and the reference value of the DC output voltage V_o is set to 200 V. According to Figure 14, when the proposed converter operates in “Buck” state and the “Buck-Boost” state, the maximum filter capacitor voltage ripple is about 22 V and 37 V respectively, which is consistent with Equations (17) and (18). Figure 15 shows the measured grid voltage ($V_g(t)$) and grid-injected current ($i_g(t)$) when the DC load changes from 154 Ω to 82 Ω . Figure 16 shows the dynamic response of V_o when the grid voltage are increased from 130 V to 220 V. It can be observed that the DC output voltage has a voltage fluctuation and the maximum DC voltage is about 210 V, which means that the dynamic response of V_o can be further optimized by using a lower time constant PI compensator in each controller.

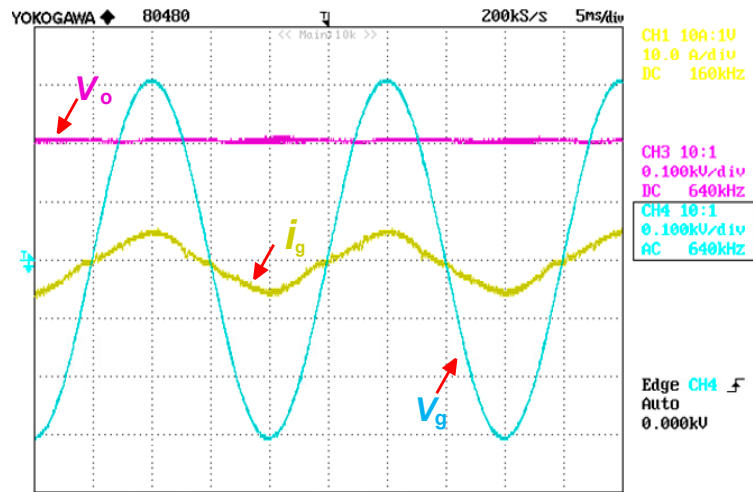


Figure 13. Measured AC grid voltage ($V_g(t)$), the DC voltage (V_o), and the input grid current i_g , when $V_o = 200$ V, $V_g = 220$ V, $R = 60 \Omega$.

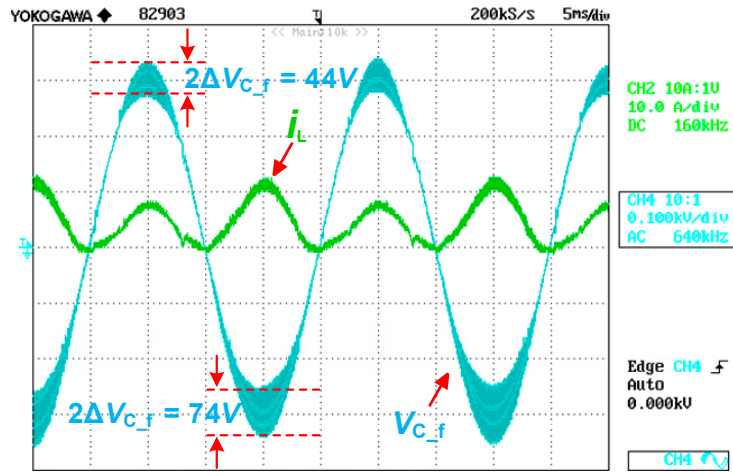


Figure 14. Measured capacitor voltage ($V_{C_f}(t)$) and the dc inductor current i_L , when $V_o = 200$ V, $V_g = 220$ V, $R = 60 \Omega$.

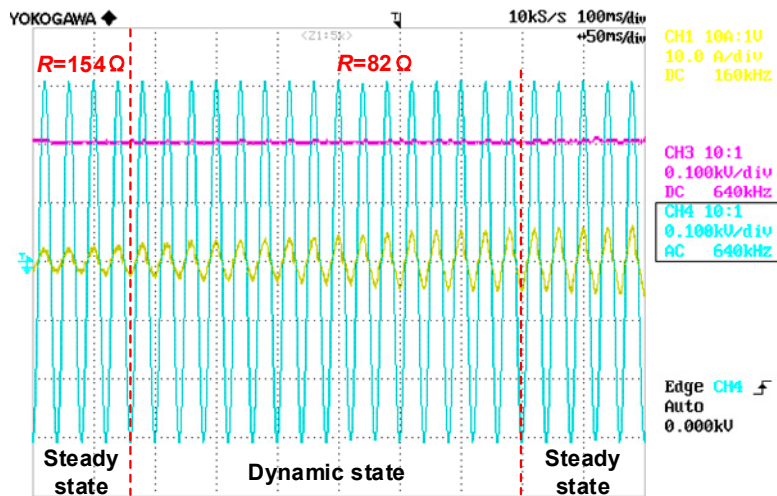


Figure 15. Measured AC grid voltage ($V_g(t)$), the DC voltage (V_o), and the input grid current i_g , when $V_o = 200$ V, $V_{gm} = 220$ V.

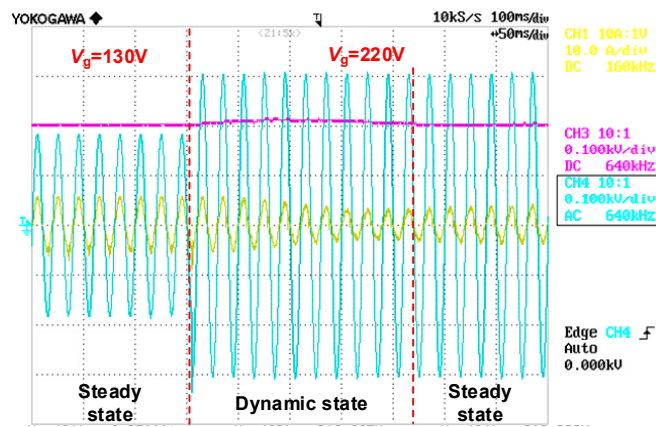


Figure 16. Measured AC grid voltage ($V_g(t)$), the DC voltage (V_o), and the input grid current i_g , when $V_o = 200\text{ V}$, $V_{gm} = 220\text{ V}$, $R = 60\ \Omega$.

Figures 17 and 18 show the measured efficiency of the converter, when the AC grid voltages are 110 V and 220 V, respectively. In addition, the measured and calculated efficiency curves versus input power of the proposed converter are plotted in Figure 19, under that the AC grid voltage is 220 V. It can be seen that the measured efficiency curve and the calculated efficiency curve have the same trend of change. Because of the additional decentralized power losses in the experiment, the calculated efficiency is higher than the measured efficiency. Figure 20 shows the calculated power losses of main devices, while P_{in} is 745 W versus the different output DC voltage V_o . It can be seen that the power losses of S_3 are larger than those of S_1 or S_2 . Moreover, although DC inductor and grid inductor use the same core EE110 and core material, the DC inductor operates at 40 kHz and the grid inductor operates at 50 Hz. The core loss increases with increasing frequency under the same core, so, the core power loss of grid inductor is much smaller than the DC inductor. In addition, there is little difference in copper loss between the two inductors at the same power. So, as shown in Figure 20, the total power losses of DC inductor are much higher than the total power losses of grid inductor and account for a large proportion of the total proposed converter power losses. Figure 21 shows the power losses distribution of semiconductor devices in “Boost”, “Buck” and “Buck-Boost” working states respectively when $V_g = 220\text{ V}$, $V_o = 200\text{ V}$ and $P_{in} = 745\text{ W}$. According to Equations (6)–(8), when the proposed converter is operated in the Buck–Boost state with the same specification, the average DC inductor current of the Buck–Boost state is larger than that of the Boost state or Buck state. Therefore, in the “Buck–Boost” state, the conduction and switching losses are higher compared to the “Buck” or “Boost” states.



Figure 17. The measured efficiency of the proposed converter when $V_g = 110\text{ V}$, $E = 200\text{ V}$, $R = 110\ \Omega$.

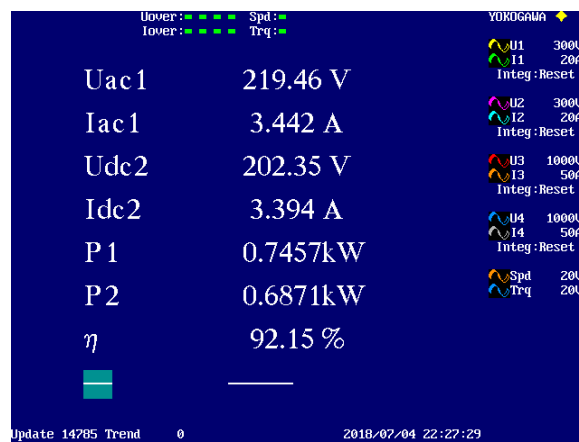


Figure 18. The measured efficiency of the proposed converter when $V_g = 220\text{ V}$, $E = 200\text{ V}$, $R = 60\ \Omega$.

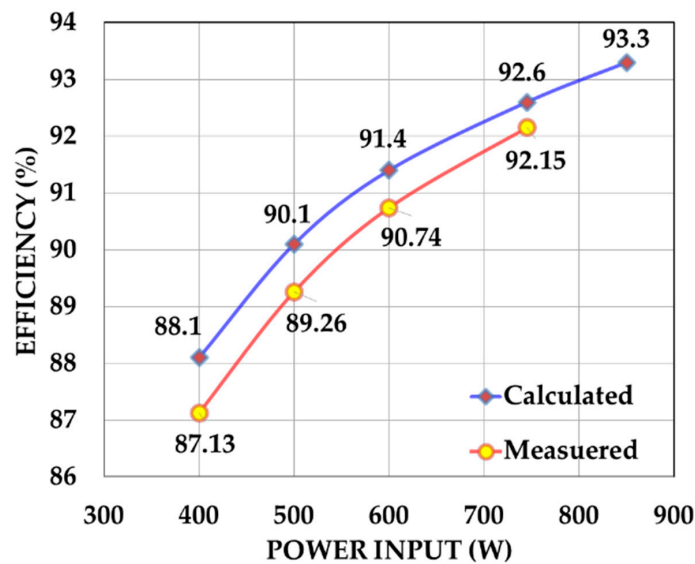


Figure 19. Calculated and measured efficiency curve of proposed converter versus the different input power when $V_g = 220\text{ V}$, $V_o = 200\text{ V}$.

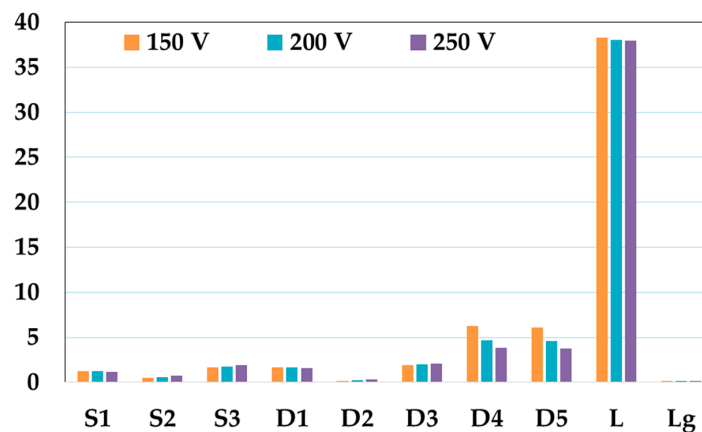


Figure 20. Power losses distribution of main devices versus the different output DC voltages when $V_g = 220\text{ V}$, $P_{in} = 745\text{ W}$.

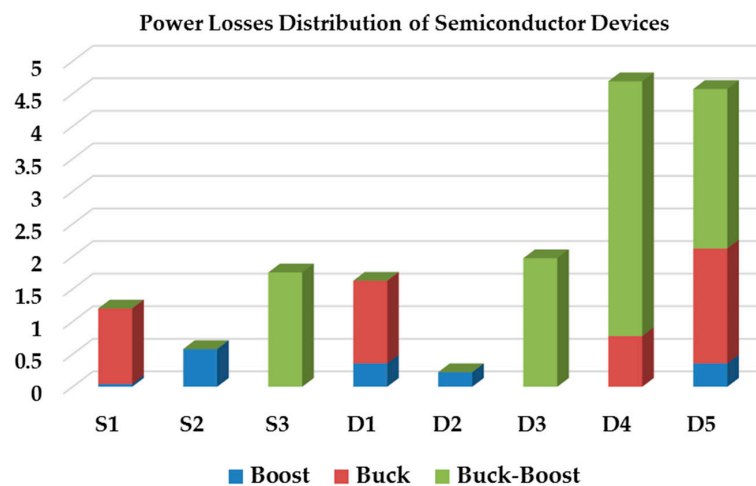


Figure 21. Power losses distribution of semiconductor devices in different working states when $V_g = 220$ V, $V_o = 200$ V, $P_{in} = 745$ W.

6. Discussion

A comparison of various features of the proposed scheme with existing Buck-Boost AC to DC converters based on united grounding configuration has been performed and presented in Table 3. It can be seen that the proposed Buck-Boost AC to DC converter has the advantage of low number of passive elements and high utilization factor of DC inductor. Compared to the converter proposed in [10], there is no problem of output-DC-voltage unbalance in the proposed AC to DC converter. Compared to the converter proposed in [12,13], the proposed Buck-Boost AC to DC converter has acceptable operating states and control strategy. Since the new AC to DC converter operates in Buck-Boost state during the negative AC grid voltage, the efficiency of the whole system is lower than the converters presented in [10,12,13]. Limited by the laboratory hardware resources, the core EE110 is adopted in DC inductor. This is another factor that affects the efficiency of the proposed converter. Using lower power losses semiconductor devices and using inductors with small core size and low core losses can improve the efficiency of the whole system. Thus, when prioritizing the low cost and small volume of the system, the proposed AC to DC converter is an optional interface device between the AC low voltage grid and the DC nano-grid.

Table 3. Comparison table of various Buck-Boost AC to DC converters based on united grounding configuration.

Topology	Converter in [10]	Converter in [12]	Converter in [13]	Proposed Converter
Switches	4	6	4	3
Diodes	6	6	6	5
Capacitor	3	3	3	2
DC inductors	2	2	2	1
Operating states	Buck, Boost	Buck, Boost, Flybuck, Flyback	Buck, Boost, Flybuck, Flyback	Buck, Boost, Buck-Boost
Utilization factor of DC inductor	50%	50–100%	50–100%	100%
Complexity of small-signal models	Three-order			
Reference DC output voltage	$V_{o_ref} = 400$ V		$V_{o_ref} = 200$ V	

Table 3. Cont.

Topology	Converter in [10]	Converter in [12]	Converter in [13]	Proposed Converter
$V_g = 110\text{V}$.	Loads	$R_{L1} = 144 \Omega, R_{L2} = 94 \Omega$		$R = 110 \Omega$
	V_{o1}	223.67 V	200.86 V	200.90 V
	V_{o2}	-176.43 V	-198.69 V	-198.61 V
	Efficiency	95.45%	92.96%	93.37%
$V_g = 220\text{V}$.	Loads	$R_{L1} = 72 \Omega, R_{L2} = 52 \Omega$.		$R = 60 \Omega$
	V_{o1}	221.08 V	203.33 V	202.94 V
	V_{o2}	-179.37 V	-196.14 V	-197.35 V
	Efficiency	96.24%	96.22%	96.33%

7. Conclusions

A new transformerless Buck-Boost AC to DC converter is adopted as an interface between the AC low voltage grid and the DC nano-grid. The characteristics of this converter can be summarized as following:

1. Similar to the Buck-Boost AC to DC converter presented in [10,12,13], the same ground line can be used by the AC grid and DC nano-grid without any transformer isolation, which ensures the earth-fault protection for a hybrid power system.
2. Different from the Buck-Boost AC to DC converter presented in [10,12,13], only a single DC inductor and fewer switching devices are adopted, which can reduce the costs and volume of the system. The utilization factor of DC inductor is 100%, but it should be noted that the efficiency of the new AC to DC converter has been affected, since the new converter operates in Buck-Boost state during the negative AC grid voltage.

The principle of proposed converter has been described through the equivalent circuits. Experimental results obtained from a 220 V/50 Hz/800 W prototype have verified the feasibility and effectiveness of the proposed AC to DC converter.

How to improve the efficiency of this converter should be focused on for next step research, for example, replacing the diodes with the MOSFETs to reduce the conduction power losses or replacing the material of the inductor core with low power loss to reduce the inductor power losses.

Author Contributions: Conceptualization, X.L., W.W. and H.W.; methodology, X.L., W.W. and N.G.; software, X.L. and H.W.; validation, X.L., and N.G.; formal analysis, H.W. and W.W.; investigation, X.L. and H.W.; resources, W.W.; data curation, X.L.; writing—original draft preparation, X.L., W.W., H.W., H.S.-h.C. and F.B.; writing—review and editing, X.L., W.W., H.W., H.S.-h.C. and F.B.; visualization, X.L.; supervision, W.W.; project administration, W.W.; funding acquisition, W.W.

Funding: This work was supported in part by NSFC under Grant 51577114, in part by Shanghai Municipal Education Committee under Grant 14SG43, and in part by the Shanghai Science and Technology Commission under Grant 17040501500.

Conflicts of Interest: The authors declare no conflict of interest.

Nomenclature

i_g	Grid current
I_{g_peak}	Peak amplitude of grid current
v_g	Grid voltage
V_{g_peak}	Peak amplitude of grid voltage
ω	Angular frequency of grid
v_{C_f}	Voltage across the filter capacitor

v_o	DC output voltage
D_{Boost}	Duty ratio in “Boost” state
D_{Buck}	Duty ratio in “Buck” state
$D_{Buck-Boost}$	Duty ratio in “Buck-Boost” state
i_L	Low frequency DC inductor current
v_L	Voltage across the DC inductor
L	Value of DC inductor
Δi_L	Current ripple of the DC inductor
T_{ON}	Turn-on time in a switching period
T_{OFF}	Turn-off time in a switching period
f_{SW}	Switching frequency
Δi_{L_Boost}	DC inductor current ripple in “Buck” state
Δi_{L_Buck}	DC inductor current ripple in “Boost” state
$\Delta i_{L_Buck-Boost}$	DC inductor current ripple in “Buck-Boost” state
i_{C_f}	Current of filter capacitor
C_f	Value of filter capacitor
Δv_{C_f}	Voltage ripple peak to peak value of the filter capacitor
$\Delta v_{C_f_Buck}$	Voltage ripple peak to peak value of the filter capacitor in “Buck” state
$\Delta v_{C_f_Buck-Boost}$	Voltage ripple peak to peak value of the filter capacitor in “Buck-Boost” state
D_{S1}	Duty cycle of the switch S_1
D_{S3}	Duty cycle of the switch S_3

References

1. Sannino, A.; Postiglione, G.; Bollen, M.H.J. Feasibility of a DC network for commercial facilities. *IEEE Trans. Ind. Appl.* **2003**, *39*, 1499–1507. [[CrossRef](#)]
2. Salomonsson, D.; Sannino, A. Low-voltage DC distribution system for commercial power systems with sensitive electronic loads. *IEEE Trans. Power Deliv.* **2007**, *22*, 1620–1627. [[CrossRef](#)]
3. Sathyan, S.; Suryawanshi, H.M.; Shitole, A.B.; Ballal, M.S.; Borghate, V.B. Soft Switched Interleaved DC/DC Converter as front-end of Multi Inverter Structure for Micro Grid Applications. *IEEE Trans. Power Electron.* **2018**, *33*, 7645–7655. [[CrossRef](#)]
4. Kinhekar, N.; Padhy, N.P.; Li, F.; Gupta, H.O. Utility Oriented Demand Side Management Using Smart AC and Micro DC Grid Cooperative. *IEEE Trans. Power Syst.* **2016**, *31*, 1151–1160. [[CrossRef](#)]
5. Prabhakaran, P.; Goyal, Y.; Agarwal, V. Novel Nonlinear Droop Control Techniques to Overcome the Load Sharing and Voltage Regulation Issues in DC Microgrid. *IEEE Trans. Power Electron.* **2018**, *33*, 4477–4487. [[CrossRef](#)]
6. Xu, Q.; Hu, X.; Wang, P.; Xiao, J.; Tu, P.; Wen, C.; Lee, M. A Decentralized Dynamic Power Sharing Strategy for Hybrid Energy Storage System in Autonomous DC Microgrid. *IEEE Trans. Ind. Electron.* **2017**, *64*, 5930–5941. [[CrossRef](#)]
7. Yue, X.; Boroyevich, D.; Lee, F.C.; Chen, F.; Burgos, R.; Zhuo, F. Beat Frequency Oscillation Analysis for Power Electronic Converters in DC Nanogrid Based on Crossed Frequency Output Impedance Matrix Model. *IEEE Trans. Power Electron.* **2018**, *33*, 3052–3064. [[CrossRef](#)]
8. Yang, Q.; Jiang, L.; Zhao, H.; Zeng, H. Autonomous Voltage Regulation and Current Sharing in Islanded Multi-inverter DC Microgrid. *IEEE Trans. Smart Grid* **2018**, *9*, 6429–6437. [[CrossRef](#)]
9. Cai, W.; Jiang, L.; Liu, B.; Duan, S.; Zou, C. A Power Decoupled Method Based on Four-Switch Three-Port DC/DC/AC Converter in DC Microgrid. *IEEE Trans. Ind. Appl.* **2015**, *51*, 336–343. [[CrossRef](#)]
10. Wu, W.; Wang, H.; Liu, Y.; Huang, M.; Blaabjerg, F. A Dual-Buck-Boost AC/DC Converter for DC Nanogrid with Three-Terminal Outputs. *IEEE Trans. Ind. Electron.* **2017**, *64*, 295–299. [[CrossRef](#)]
11. Rivera, S.; Wu, B.; Kouro, S.; Yaramasu, V.; Wang, J. Electric Vehicle Charging Station Using a Neutral Point Clamped Converter With Bipolar DC Bus. *IEEE Trans. Ind. Electron.* **2015**, *62*, 1999–2009. [[CrossRef](#)]
12. Wang, H.; Wu, W.; Li, Y.W.; Blaabjerg, F. A Coupled-Inductor-Based Buck-Boost AC/DC Converter with Balanced DC Output Voltages. *IEEE Trans. Power Electron.* **2019**, *34*, 151–159. [[CrossRef](#)]
13. Wang, H.; Wu, W.; Gao, N.; He, Y.; Chung, H.S.; Blaabjerg, F. Modified dual buck-boost AC/DC converter with self-balanced DC output voltages. *IET Power Electron.* **2019**, *12*, 1170–1178. [[CrossRef](#)]

14. Park, J.D.; Candelaria, J. Fault Detection and Isolation in Low-Voltage DC-Bus Microgrid System. *IEEE Trans. Power Deliv.* **2013**, *28*, 779–787. [[CrossRef](#)]
15. Salomonsson, D.; Soder, L.; Sannino, A. Protection of Low-Voltage DC Microgrids. *IEEE Trans. Power Deliv.* **2009**, *24*, 1045–1053. [[CrossRef](#)]
16. Singh, B.; Singh, B.N.; Chandra, A.; Al-Haddad, K.; Pandey, A.; Kothari, D.P. A review of single-phase improved power quality AC-DC converters. *IEEE Trans. Ind. Electron.* **2003**, *50*, 962–981. [[CrossRef](#)]
17. Singh, B.; Singh, B.N.; Chandra, A.; Al-Haddad, K.; Pandey, A.; Kothari, D.P. A review of three-phase improved power quality AC-DC converters. *IEEE Trans. Ind. Electron.* **2004**, *51*, 641–660. [[CrossRef](#)]
18. Jovanovic, M.M.; Jang, Y. State-of-the-art, single-phase, active power-factor-correction techniques for high-power applications—An overview. *IEEE Trans. Ind. Electron.* **2005**, *52*, 701–708. [[CrossRef](#)]
19. Kolar, J.W.; Friedli, T. The Essence of Three-Phase PFC Rectifier Systems—Part I. *IEEE Trans. Power Electron.* **2013**, *28*, 176–198. [[CrossRef](#)]
20. Friedli, T.; Hartmann, M.; Kolar, J.W. The Essence of Three-Phase PFC Rectifier Systems—Part II. *IEEE Trans. Power Electron.* **2014**, *29*, 543–560. [[CrossRef](#)]
21. Wu, W.; Liu, Y.; Wang, H.; Huang, M.; Blaabjerg, F. Modelling and control design of a dual Buck-Boost AC/DC converter used in the DC Nano-grid. In Proceedings of the IEEE 8th International Power Electronics and Motion Control Conference (IPEMC-ECCE Asia), Hefei, China, 22–26 May 2016; pp. 2187–2192.
22. Liu, Y.; Wu, W.; He, Y.; Lin, Z.; Blaabjerg, F.; Chung, H.S. An Efficient and Robust Hybrid Damper for LCL- or LLCL-based Grid-Tied Inverter with Strong Grid-side Harmonic Voltage Effect Rejection. *IEEE Trans. Ind. Electron.* **2016**, *63*, 926–936. [[CrossRef](#)]
23. Wang, J.; Yan, J.D.; Jiang, L.; Zou, J. Delay-Dependent Stability of Single-Loop Controlled Grid-Connected Inverters with LCL Filters. *IEEE Trans. Power Electron.* **2016**, *31*, 743–757. [[CrossRef](#)]
24. Wang, H.; Wu, W.; Zhang, S.; He, Y.; Chung, H.S.; Blaabjerg, F. A modified Aalborg inverter extracting maximum power from one PV array source. *CPSS Trans. Power Electron. Appl.* **2019**, *4*, 109–118. [[CrossRef](#)]
25. Fang, J.; Li, X.; Yang, X.; Tang, Y. An Integrated Trap-LCL Filter with Reduced Current Harmonics for Grid-Connected Converters Under Weak Grid Conditions. *IEEE Trans. Power Electron.* **2017**, *32*, 8446–8457. [[CrossRef](#)]
26. Wu, W.; Liu, Y.; He, Y.; Chung, H.S.; Liserre, M.; Blaabjerg, F. Damping Methods of Resonances Caused by LCL-Filter-Based Current-Controlled Grid-tied Power Inverters: An Overview. *IEEE Trans. Ind. Electron.* **2017**, *64*, 7402–7413. [[CrossRef](#)]



© 2019 by the authors. Licensee MDPI, Basel, Switzerland. This article is an open access article distributed under the terms and conditions of the Creative Commons Attribution (CC BY) license (<http://creativecommons.org/licenses/by/4.0/>).